Research Article
Vol. 29, No. 7 / 29 March 2021 / *Optics Express* 10150
Optics EXPRESS

Exploiting the single-photon detection performance of InGaAs negative-feedback avalanche diode with fast active quenching

JUNLIANG LIU,[1,2] YINING XU,[2] YONGFU LI,[2,3,*] ZHAOJUN LIU,[1,2] AND XIAN ZHAO[2,3]

[1] *School of Information Science and Engineering, Shandong University, 72 Binhai Road, Qingdao 266237, China*
[2] *Key Laboratory of Laser & Infrared System (Shandong University), Ministry of Education, 72 Binhai Road, Qingdao 266237, China*
[3] *Center for Optics Research and Engineering, Shandong University, 72 Binhai Road, Qingdao 266237, China*
[*] *yfli@sdu.edu.cn*

Abstract: InGaAs/InP-based negative-feedback avalanche diodes (NFADs) for 1550 nm single-photon detection with easy-to-use and low-afterpulsing features have attracted many researchers on lidar and quantum optics. Here we present a fast active-quenching circuit specifically designed to exploit the performance of a multi-mode fiber coupled NFAD for free-running operation by a further suppression on afterpulsing effects. The quenching and recovery processes of the device were characterized using electroluminescent method and a novel dual-pulse method, respectively. Results show that the proposed circuit was capable of reducing the time required for quenching and recovery process of the NFAD by approximately 20 ns, and contributed to a reduction in the number of avalanche carriers by up to 30%. As a result, the total afterpulse probability (TAP) of the NFAD with active quenching was reduced by up to 70% compared with the condition without active quenching, and by approximately 90% compared with a standard InGaAs SPAD at the photon detection efficiency (PDE) of 20%. The TAP of the proposed detector was lower than 11% when the dead time was longer than 200 ns, 600 ns, and 2 μs at the PDE of 10%, 15%, and 25%, respectively, and the usable dead time was down to 80 ns with a TAP of 20.4% at the PDE of 10%, 1550 nm, 223 K, where the DCR was as low as 918 Hz. The low-afterpulsing, low-dead-time, low-DCR features of this compact detector makes it especially suitable for use in lidar applications.

1. Introduction

Eye-safe lidar has become an hot topic in recent years. For long-range lidar applications with eye-safe requirements, a preferred option is using 1.55 μm laser because of its higher power allowance and lower atmospheric loss [1,2]. However, the detection of 1.55 μm photons is not similarly convenient as the detection of photons of below 1 μm. Photo-multiplier tubes sensitive to 1.55 μm photons have a low detection efficiency and high dark counts. Superconducting nanowires have demonstrated superb overall performance, especially with a detection efficiency of as high as 95% [3] at 1.55 μm, but the requirement of extremely low working temperature prohibits its use in size-limited mobile applications. Up-conversion single-photon detector has shown a maximum detection efficiency up to 40% with a noise counting rate of 200 cps at 1550 nm, but is only available with single-mode fiber [4]. Recently, Ge-on-Si single-photon avalanche diode (SPAD) has demonstrated a low-cost and high-performance approach for near-infrared lidar application [5], but still require cryostats for a low dark count rate [6,7].

#420368
Journal © 2021
https://doi.org/10.1364/OE.420368
Received 22 Jan 2021; accepted 9 Mar 2021; published 16 Mar 2021

InGaAs/InP SPAD gains popularity in lidar applications since an efficient reception of the echo photons at 1.55 μm has been achieved with multi-mode fiber coupling [8], following its wide use in quantum communication systems [9]. It requires only thermoelectric cooling for normal operation in lidar system, and thus has a small size and low power consumption. Since the avalanche process in SPADs cannot cease by itself, several electronic techniques were developed to quench it, and then reset the SPAD for the next detection [9,10]. Among all techniques, fast passive quenching with locally placed large resistor [11,12] and fast active quenching [13,14] have enabled free-running single-photon detection with InGaAs SPADs.

In particular, free-running single-photon detectors based on negative-feedback avalanche diodes (NFADs) are favored by lidar researchers and users because of its compactness and multi-mode fiber coupling [8]. The NFAD integrates a thin-film resistor at the anode of the SPAD to minimize the delay in passive quenching, and hence greatly reduces avalanche carriers and lessens afterpulsing effects that may introduce false counts after a detection [15]. Unlike standard SPADs under free-running scheme, NFADs theoretically do not require an external active quenching and/or reset circuit for normal operation, as they can complete the quenching and reset process through the integrated resistor. In fact, easy-to-use is one of the most attractive features of NFADs. Without the need of placing a complicated, heat-dissipating active-quenching circuit as close as possible, NFAD can be further cooled to have only 1 dark count per second at 10% detection efficiency [16]. Note that it is still necessary to serve active reset to the NFAD when arbitrary hold-off time or gated operation is in demand. Using operational amplifier and field-programmable gate array (FPGA), researchers have managed to prolong the dead time of the NFAD to obtain even lower afterpulse probability [11,17].

The large quenching resistor of the NFAD is a double-edged sword. The minimum dead time of the SPAD is set by the time required to recharge the junction capacitor, and the integrated large resistor leads to a significantly longer recovery time of the NFAD, typically around 200 ns [18,19], compared with the sub-nanosecond scale for a typical InGaAs SPAD. In applications such as aerosol lidar, low dead time is necessary to avoid count saturation [17]. Sanzaro et al. developed InGaAs/InP SPADs with integrated zinc-diffused resistors of smaller resistance values to achieve approximately 50 ns recovery time [12], where external active quenching should be applied to complete quenching due to the insufficient resistance of the quenching resistors. However, none of the researchers has characterized the behavior of the NFAD under fast active quenching.

In this paper, a fast active-quenching circuit was designed to further exploit the performance of the NFAD. The quenching process of the NFAD was characterized using electroluminescent method, and a dual-pulse detection method was proposed to characterize the recovery process and the dead time. The performance of the NFAD was then evaluated, including afterpulse probability and dark count rate at various conditions of detection efficiency and dead time. All the measurements of the NFAD were conducted under the conditions with and without active quenching. Furthermore, the NFAD is compared with a standard SPAD wit the same multi-mode fiber coupling, in terms of the quenching process and the performance.

2. Circuit design and modeling

An active-quenching circuit was specially designed for the NFAD, shown in Fig. 1. The circuit was proposed with the aim to minimize the quenching and recovery time while keeping the easy-to-use feature of the NFAD. This design concept makes the circuit different from our previous work [14] which require the NFAD to be placed as close as possible to the circuit, and thus more cooling schemes and flexible uses are allowed.

Unlike standard SPADs, the NFAD needs an amplifier to pick up its avalanche current [20], which leads to an inevitable increase in the quenching delay compared with typical fast active-quenching circuits [14,21]. A high-bandwidth fully-differential amplifier (FDA) was selected in our design for avalanche current pick-up and the rejection of noise generated by the transient

Optics EXPRESS

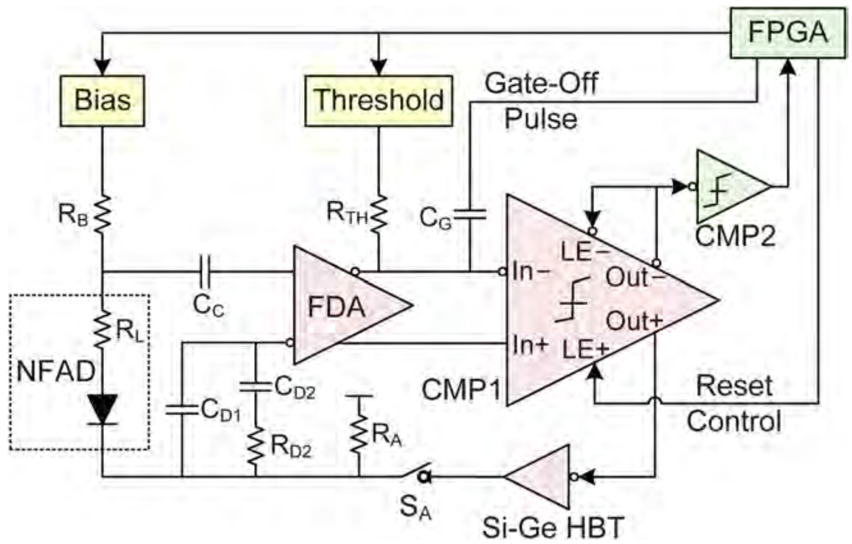

Fig. 1. Simplified schematic of the active-quenching circuit. LE: latch enable. FDA: fully-differential amplifier. CMP: comparator.

response of the reset signal. The avalanche current flows through the integrated resistor R_L, and is picked up by the FDA through AC-coupling with C_C. The bandwidth of the FDA is 1.8 GHz and the feedback resistor is 1 kΩ. Since the amplitude of the avalanche pulse is typically larger than 1 mV on 50Ω without amplifier [22], the pulse amplitude at the output of the FDA is at least 20 mV, which is sufficiently large for discrimination. An external RC network composed of C_{D1}, C_{D2}, and R_{D2} is placed between the cathode to produce a transient response of the reset signal, which is sent to non-inverting input of the FDA to cancel the similar response output from the SPAD. The amplified avalanche pulse is sent to an ultra-fast SiGe comparator (CMP1) to be discriminated. When an avalanche pulse is detected, the positive output of CMP1 is inversely amplified by a silicon-germanium hetero-junction bipolar transistor (SiGe HBT) to lower the voltage at the cathode of NFAD by approximately 4 V for the quenching of NFAD. Meanwhile, the inverting latch enable (LE-) pin of CMP1 is pulled low by the inverting output of CMP1, and CMP1 is latched to hold the quenched state. The inverting output of CMP1 is also sent to the FPGA for data acquisition after being buffered by another comparator (CMP2). The total quenching delay of the circuit is approximately 785 ps, where the delay of the FDA, CMP1, HBT and routing are about 400 ps, 85 ps, 200 ps, and 100 ps, respectively.

In order to compare the results with and without active quenching, a jumper S_A made of a removable tiny piece of solder is inserted between the cathode of NFAD and the HBT. When S_A is open, the excess bias is always applied to the cathode of NFAD through a resistor R_A of 50Ω; otherwise, active quenching is enabled.

The hold-off time is programmable with the FPGA when active-quenching is in use. The time for the FPGA to process the avalanche event and send out the reset signal is 18 ± 2.5 ns, which is also the minimum hold-off time. When the hold-off time elapses, the FPGA pull the non-inverting latch enable (LE+) pin of CMP1 lower than LE- pin to unlatch CMP1, and NFAD starts recovery process. During this process, the FPGA asserts the LE+ pin of CMP1 for 15 ns to keep CMP1 latched again to enforce a stable reset process, where the residual transient response of reset pulse is temporally filtered out. As the NFAD requires more than 15 ns to recover from quenched state, the 15-ns latch time is risk-free. As a result, the minimum dead time determined by the electronics is 35 ns when active quenching is activated. The latch time could be set longer

Optics EXPRESS

if the SPAD is located away from the circuit. Besides, the NFAD can be turned off by sending a gate-off signal from the FPGA through C_G to the CMP1, which enables gated operation of the NFAD. It should be noted that the effect of quenching, reset, or gating is closely related to the internal quenching resistor and parasitic capacitance, which is discussed in the following paragraphs.

The functional model of NFAD without active quenching has been previously proposed by Itzler et al. [22]. When an avalanche is triggered, the avalanche current starts to flow from the cathode towards the anode and through the integrated quenching resistor R_L and its parasitic capacitance C_L, as shown in Fig. 2(a). As the avalanche current grows, the voltage at the anode of the SPAD increases. As a result, the effective bias voltage across the SPAD decreases, and the junction capacitor C_D starts to discharge. The discharging current flows through the SPAD as part of the total avalanche current, but it is not output. It was pointed out by Itzler et al. [22] that there is a persistent current flow before the NFAD reaches a complete spontaneous quenching. The persistent current flow has an oscillatory behavior that originates from the dynamic change of the voltage across the SPAD due to the feedback of the quenching resistor [23]. However, when active quenching is enabled, the voltage at the cathode (V_{QR}) of the NFAD is lowered promptly, and it is impossible for the junction capacitor to recharge before an active reset, which prevents the oscillatory persistent current. Thus, a complete quenching can be achieved before the original spontaneous process, where active quenching remains true to its name.

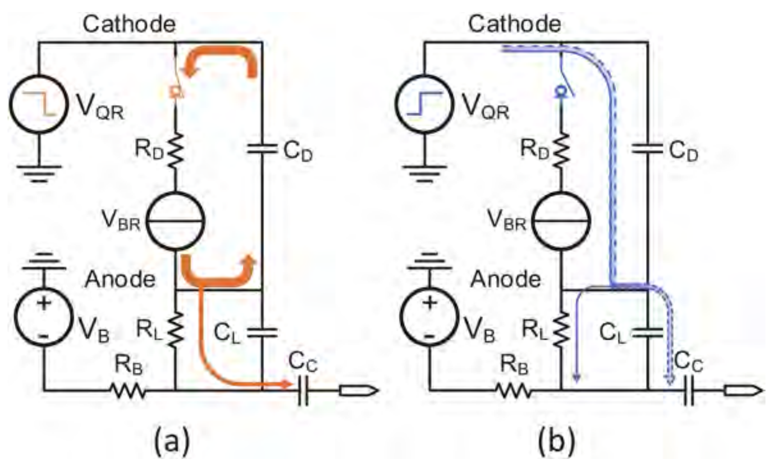

Fig. 2. Model of (a) quenching and (b) recovery process of the NFAD. V_B is the DC negative bias voltage for the NFAD. V_{QR} is a dynamic voltage source representing active quenching/reset signal at the cathode of the NFAD.

As for recovery, unlike typical SPADs, the NFAD has an integrated spiral thin-film resistor with large resistance and small parasitic capacitance, making its reset behavior different from typical SPADs under similar active-quenching scheme. For a typical SPAD driven by active-quenching active-reset circuit, the junction capacitor is recharged directly by a transistor with low output impedance. But for The NFAD shown in Fig. 2(b), C_D gets charged through both R_L and C_L as V_{QR} rises. Initially, C_D is charged through C_L until its voltage reaches

$$V_D = V_B + \frac{C_L V_{QR}}{C_D + C_L}, \tag{1}$$

and this process lasts until the rising time of V_{QR} elapses. Meanwhile, C_D is charged through R_L until it is fully charged to $V_D = V_B + V_{QR}$, and the time constant of the process is determined by $\tau = R_L C_D$, which is typically tens of nanoseconds for the NFAD [18]. It should be noted that C_D

Optics EXPRESS

is charged only through R_L for standalone operation of the NFAD without active reset, since the voltage at the cathode is a constant DC voltage.

3. Experimental setup

Before performance evaluation, the quenching and recovery process of the NFAD driven by the proposed active-quenching circuit are first to be characterized. The characterization of quenching process is through the analysis of avalanche current waveforms under standalone and active-quenching operation of the NFAD. Traditionally the waveform is amplified by a broadband radio-frequency (RF) amplifier, and is acquired by an oscilloscope. However, in order to measure the waveform without probe insertion when active quenching is activated, electroluminescent method is adopted [21]. A time-correlated single-photon counter (TCSPC) is used to record the time difference between the detection output of the NFAD and the output of another single-photon detector which detects the electroluminescent photons generated by NFAD current flow, and hence the recorded histogram represents the avalanche waveform. In this work, electroluminescent photons generated by dark counts of the NFAD are measured by using our previously built InGaAs single-photon detector, and a high-resolution low-jitter time-to-digital converter (quTAG, quTools) act as the TCSPC for the measurement.

The recovery process of the NFAD is demonstrated by the recovery of photon detection efficiency (PDE) as a function of time after the previous avalanche. Jiang et al. [18] measured the amplitude of the second pulse of a consecutive pair of dark avalanche pulses, and the amplitude as a function of pulse-arriving interval was believed to have indicated the recovery process. However, the experiment makes use of consecutive pair of dark counts, where the second pulse is probably an afterpulse due to the high afterpulse probability of InP-based devices. As a result, the measurement actually included the amplitude of dark counts and afterpulses. Besides, as indicated by the same group of researchers, the amplitude of the avalanche pulse is not always proportional to the actual excess bias or PDE of the SPAD [22]. Sanzaro et al. [12] proposed an improved method using continuous-wave laser as the source of photon flux under gated operation for their self-quenching device, and demonstrated the true photon-count recovery transient. By using this method, it is possible to derive the time needed for recovery. But the result does not include the time needed to finish the quenching process, and hence it is not possible to obtain the true dead time of the NFAD with gated operation.

Here we propose a dual-pulse method to characterize the recovery process. The principle of the method can be briefly described as follows. Pairs of laser pulses with adjustable interval are attenuated to be the temporal photon-pair source for detection using the NFAD under test. A TCSPC records all the count events, but the detection event of the second photon is regarded valid only when the first photon of the pair is also detected. Thus, as the time interval between the two photons in the pair increases, the number of valid counts of the second photon rises accordingly with the recovery of SPAD, until the interval is longer than the time needed for recovery. By using this method, it is possible to obtain the true dead time rather than merely recovery time after active reset if activated, and the process is evaluated in terms of PDE rather than pulse amplitude.

A test bench based on FPGA is built for the proposed method, shown in Fig. 3. A time-to-digital converter (TDC) with 36 ps resolution and 3.75 ns dead time is embedded in the FPGA for the event timing and recording, and the data are transmitted to a computer through USB 3.0. The photon source used in the experiment is an externally triggered 1550 nm pulsed laser diode (PDL 800-B, PicoQuant), and the output laser pulse is attenuated to 1 photon per pulse on average. The laser trigger signal is composed of electric pulse pairs with a fixed repetition frequency of 50 kHz, generated by the FPGA. The interval of the electric pulse pair is adjustable from 24 ns to 512 ns with 1 ns step. The trigger of only the first pulse of each pulse pair is copied as the synchronized start signal for the TDC. By using this test bench, the recovery process can be readily recorded.

Optics EXPRESS

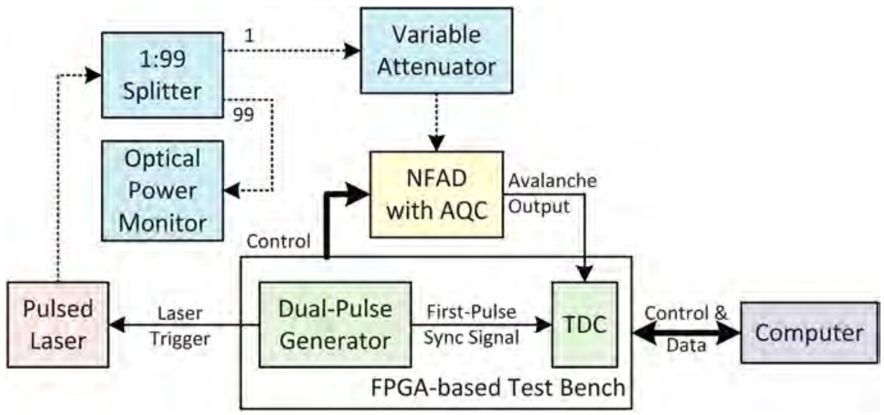

Fig. 3. The experimental setup for recovery characterization and performance evaluation of the proposed detector. NFAD: negative-feedback avalanche diode. TDC: time-to-digital converter. AQC: the proposed active-quenching circuit. The dashed lines represent single-mode optical fibers, not including the pig-tailed multi-mode fiber of the NFAD, and the solid lines represent coaxial electrical connections.

The InGaAs/InP NFAD under test in this work is PNA-300-MM from RMY Electronics, which inherits the NFAD technology from Princeton Lightwave. The device is coupled with 62.5 μm multi-mode fiber, making it suitable for use in lidar systems. In addition, the avalanche waveform and single-photon detection performance of a standard InGaAs/InP SPAD (PGA-314-62.5, RMY Electronics) with the same 62.5 μm multi-mode fiber coupling were also measured as a comparison, driven by our state-of-the-art active-quenching circuit designed for standard SPADs [14]. Both of the devices share the same response to 1550 nm light as 0.65 A/W at M = 1.

The performance of the device is mainly characterized by dark count rate and afterpulse probability as a function of PDE and dead time. The aforementioned TCSPC system and laser source were used in the experiments, but the laser was triggered by a single-pulse signal with a repetition rate of 39 kHz, and was attenuated to 0.1 photon per pulse on average for performance evaluation experiments.

The raw dark count rate (C_{dr}) at different photon detection efficiencies and hold-off times can be directly measured without illumination. However, taking dead time (τ_d) into consideration, the compensated dark count rate (DCR, C_d) can be calculated by the following equations [24]:

$$C_d = \frac{C_{dr}}{1 - \tau_d C_{dr}}. \tag{2}$$

Afterpulse probability is typically characterized in two ways. The first way is to demonstrate the temporal evolution of the afterpulse probability, i.e., the afterpulse probability density. Double-gated method is often adopted for the measurement of afterpulse probability [25], with a gate width of nanosecond scale. However, as it is difficult to apply a gate with precise width and opening timing to the NFAD due to its long recovery time, the measurement was performed under free-running operation in this work, which included higher-order afterpulsing effect [26]. For the circumstance mentioned above, the afterpulse probability density (P_{ap}) as a function of time t after an avalanche event can be calculated by:

$$P_{ap}(t) = \frac{C(t) - \tau_b C_{dr}}{\tau_b (C_i - \tau_w C_{dr})}, \tag{3}$$

where $C(t)$ is the count rate within the time bin at time t in the histogram, C_{dr} is the raw dark count rate, τ_w is the width of the illuminated time window, C_i is the count rate within the illuminated time window.

The other way is to evaluate total afterpulse probability (TAP, P_{tap}), which represents the total number of afterpulses a previous avalanche event can trigger on average. Since $P_{ap}(t)$ is already calculated under free-running scheme rather than gated mode, the TAP can be calculated simply by integrating $P_{ap}(t)$ from the end of dead time to the end of laser period.

4. Results and discussion

In this section, all results for the NFAD were obtained by enabling and disabling the active quenching function, and are abbreviated as “with AQ” and “without AQ”, respectively. All values of photon detection efficiency mentioned in this section were measured at 1550 nm.

Typical avalanche waveforms of the NFAD are shown in Fig. 4(a), represented by the number of electroluminescent photons per 1000 avalanche events as a function of time at an excess bias of 2.5 V, 223 K. The dead time of the start channel of the TCSPC was set to 200 ns to avoid restart of timing due to afterpulsing.

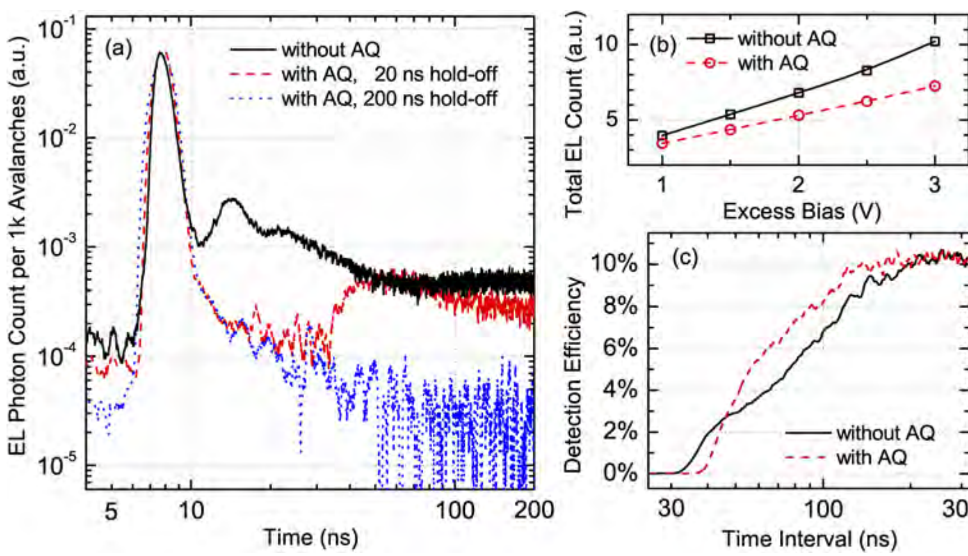

Fig. 4. (a) Avalanche waveforms of the NFAD at an excess bias of 2.5 V, 223 K, under the following quenching conditions: without active quenching, with active quenching and 20 ns hold-off time, and with active quenching and 200 ns hold-off time. The waveforms are demonstrated by their electroluminescent photon counts per 1000 avalanches. (b) Total electroluminescent photon count as a function of excess bias, . (c) Transition of recovery process, demonstrated by photon detection efficiency (PDE) as a function of time interval between the detection of the first photon and the second one, at a nominal PDE of 10%, 223 K. EL: electroluminescent. AQ: active quenching.

In general, it takes approximately 1 ns for the resistor to effectively lower the avalanche current by one order of magnitude. And then, with only passive quenching by the integrated resistor, there is at least one secondary current peak within 20 ns after the main peak. This behavior without AQ has been explained by Hayat [27], Ramirez [23], et al., where dynamic coupling between the voltage across the SPAD, the feedback from the integrated resistor and the impact ionization process were considered to be the reasons.

Optics EXPRESS

However, when active quenching was enabled, the behavior of NFAD changed apparently. First of all, the second peak disappears. This phenomenon clearly shows that the recharge of the junction capacitor and consequently the secondary avalanches (i.e. small peaks) were suppressed by lowering the bias actively and promptly. Compared with the waveform without AQ, the time required for a complete quenching was shortened by approximately 20 ns. Second, the current rose quickly with a small amplitude at approximately 30 ns after the first avalanche pulse, and yet this step also disappeared when the hold-off time was set to 200 ns. The results above indicate that the small step-up in the waveform after the beginning of reset does not belong to the first avalanche process, but is a statistical envelope waveform of stochastic afterpulses. Note that the active hold-off time was set to 20 ns after the discrimination of the avalanche pulse, and it took only 10 ns for the afterpulse probability density to reach a peak, which was much shorter than the recovery time of the NFAD.

Since the count of electroluminescent photons represents the amplitude of avalanche current, the total electroluminescent photon count is in direct proportion to the number of avalanche carriers. Figure 4(b) shows the total counts of electroluminescent photons per 1000 avalanches as a function of excess bias. The values with AQ is 18% to 30% lower than those without AQ as the excess bias rises from 1 V to 3 V, due to the prevention of the persisting oscillatory avalanche current after the main peak. The lower number in avalanche carriers.

As for recovery process, though Fig. 4(a) shows that the afterpulses appear only 30 ns after the previous avalanche, the typical time needed for a full recovery in NFADs is longer. The solid line in Fig. 4(c) shows the recovery transient for the NFAD without AQ at a PDE of 10%, 223 K. The start of the recovery process is 32 ns after the discrimination of previous avalanche, and the time constant of the recovery process is 66 ns. Nevertheless, the actual start time of recovery without AQ is probably a few ns earlier since avalanche pulses smaller than the threshold could not be discriminated, which has lead to the sharp rise at 32 ns in Fig. 4(c).

The recovery process of the NFAD with AQ is shown as the dashed line in Fig. 4(c). To our surprise, the start of the process is only delayed by less than 10 ns relative to the value without AQ, rather than the minimum hold-off time (20 ns) we set. Moreover, the effective time constant for recovery is only approximately 40 ns. Such result indicates that both active quenching and active reset are capable of accelerating the recovery process. On one hand, as is stated above, active reset recharges the junction capacitor through both C_L and R_L in Fig. 2. The initial charge current through C_L effectively rises the starting point of the following charging though R_L, and hence has increased the overall PDE during the recovery process. On the other hand, Ramirez et al. [23] has pointed out that spontaneous quenching is a stochastic event which occurs after one or more cycles of discharge and recharge of the junction capacitor, which introduces a delay of the finish of quenching. Since active quenching prevents this recharging behavior during the quenching process, the initial delay before recovery is shortened.

In general, the minimum dead time of the NFAD can be shortened by approximately 20 ns with the proposed circuit, and a significantly lower afterpulse probability could be achieved with AQ due to the reduction of avalanche carriers without the sacrifice of dead time, which has been proved by the following results.

The afterpulse probability densities at the PDE of 10%, 15%, and 20% for the NFAD are shown in Fig. 5. Here the “Time” axis refers to the time after the previous avalanche, rather than the hold-off time or the time after reset, in order to provide a more practical viewpoint.

It is easily observed that the values with AQ are temporarily higher than those without AQ at the beginning of the recovery (i.e. 40 ns to 60 ns), and this is attributed to the faster recovery with AQ described above. Following the recovery of the NFAD, the afterpulse probabilities with AQ stay below the values without AQ as expected, due to the reduction of avalanche charges. Since higher-order afterpulsing effect was included under free-running operation, there are small secondary peaks at about 100 ns, and the values decrease slower with time. The effect was

Optics EXPRESS

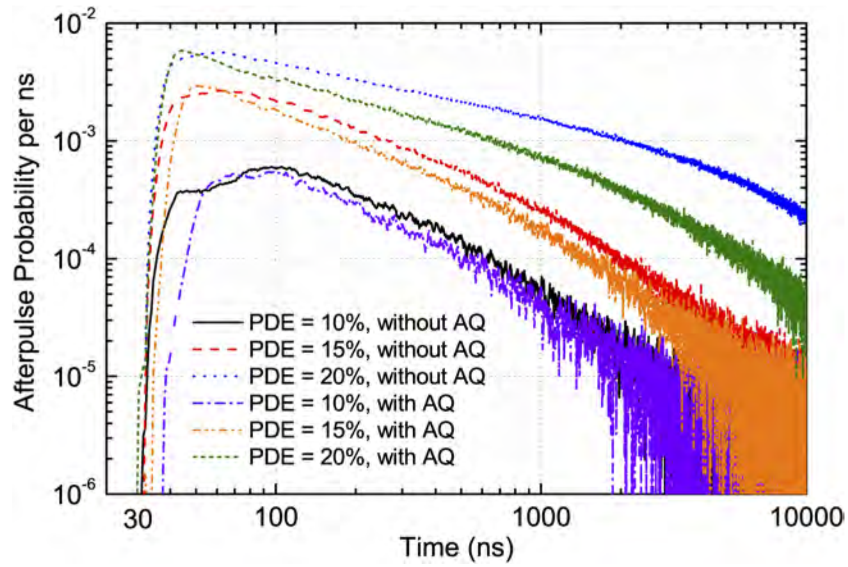

Fig. 5. Afterpulse probability per ns as a function of time after previous avalanche, at the PDE of 10%, 15%, and 20%, 223 K, with active quenching (AQ) and without AQ. The hold-off time was set to the minimum value of 20 ns for the results with AQ, and hold-off function was inactivated for the condition without AQ.

more severe without AQ, especially when the PDE was as high as 20%. In other words, more improvement on the afterpulsing performance could be achieved by using active quenching as the PDE increases.

Total afterpulse probability (TAP) is more straight-forward as an indicator of the severeness of afterpulsing effects, and is closely related to false count rate [11]. The TAP and the DCR as a function of dead time at various PDEs are shown in Fig. 6(a) and (b), respectively. Here we take the time point where the NFAD recovers 70% of its detection efficiency as the dead time. For active quenching, 60 ns should be added to the hold-off time to be the actual dead time according to the definition above, which means the minimum dead time was 80 ns. As for the conditions without AQ, the dead time was approximately 100 ns.

The solid points in Fig. 6(a) at the dead time of 100 ns are the TAP without AQ at the PDE of 10%, 15%, and 20%. The absence of the point without AQ at the PDE of 25% is due to the ultra-high count rate, which leads to an inaccurate result of TAP measurement. The TAP without AQ at 10% of PDE was slightly higher than that with AQ at 80 ns dead time and the same PDE, and the gaps between the results with and without AQ were gradually widened as the PDE increased to 20%. With AQ and proper dead time, the TAP can be suppressed to a desired degree. For example, a dead time of 200 ns, 600 ns, and 2 μs was required for a TAP of 11% at the PDE of 10%, 15%, and 25%, respectively. The TAP was 20.4% at the minimum dead time of 80 ns and the PDE of 10%. Given that a much lower distortion in the lidar signal could be expected with the 80 ns dead time, a TAP of 20.4% with a DCR as low as 918 Hz is acceptable in practical lidar application [17].

The TAP and DCR of the standard SPAD (PGA-314) were also demonstrated in Fig. 6 as a comparison. The results of the NFAD and the SPAD were similar at the PDE of 10%. Nevertheless, the NFAD started to demonstrate superior afterpulsing performance with the increase of the PDE. The TAP values of PNA-300 at the PDE of 25% were even comparable to those of PGA-314 at the PDE of 15%. At the PDE of 20%, the TAP of PNA-300 was approximately one tenth of the value of PGA-314.

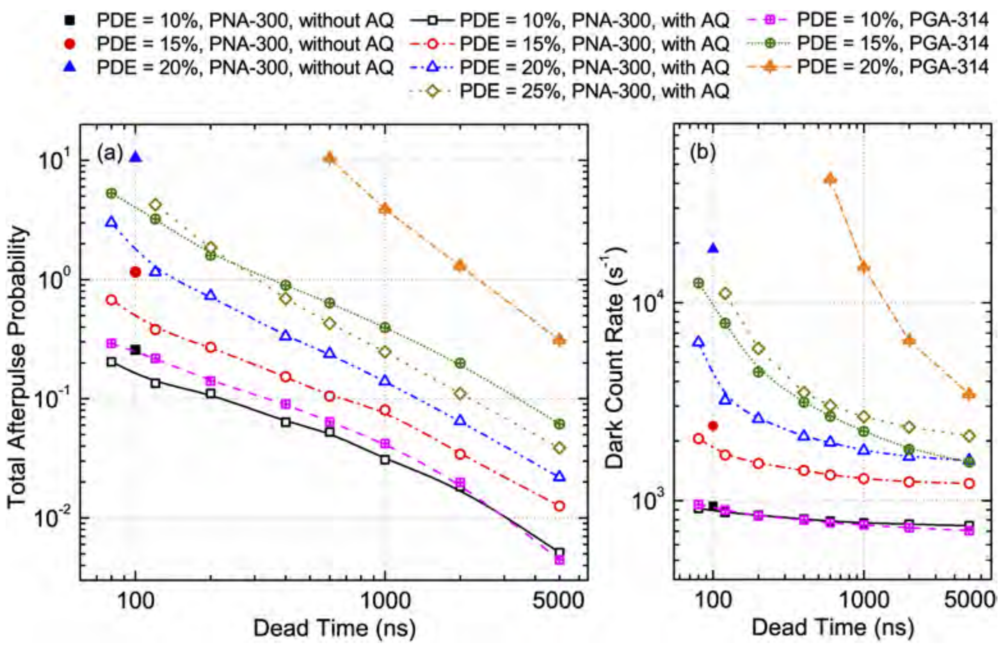

Fig. 6. Total afterpulse probability (a) and dark count rate (b) of PNA-300 (NFAD) and PGA-314 (standard SPAD) as a function of dead time at various PDEs, 223 K.

Similar trend in the DCR as that in the TAP of the devices is readily observed in Fig. 6(b), since afterpulses were included in DCR. The DCR of PNA-300 ranges from approximately 800 Hz to 10 kHz for the PDE from 10% to 25%. The DCR of PGA-314 and PNA-300 at the PDE of 10% were quite similar and were kept below 1 kHz, at the same dead time, 223 K. However, with the increase of the PDE, afterpulses contribute to a large portion of dark counts, and consequently PGA-314 shows a much higher slope of increment of the DCR compared with PNA-300.

A comparison on the avalanche waveforms and number of carriers between PNA-300 and PGA-314 is shown in Fig. 7, which can in part explain the results above. All waveforms in Fig. 7(a) and (b) were obtained using the aforementioned electroluminescent method. The faster roll-off slope in all waveforms of PGA-314 is evident in Fig. 7(b), because the active-quenching signal at the cathode of the SPAD does not have to pass through the large resistor for discharging the junction capacitor. Nevertheless, it is indicated that PNA-300 starts quenching much earlier than PGA-314. The integrated quenching resistor in PNA-300 takes effect by limiting the current while it is building up, followed by the finishing of the quenching process through active quenching. As shown in Fig. 7(c), The number of carriers of PNA-300 increased almost linearly by 31%, 75%, and 117% at the PDE of 15%, 20%, and 25%, respectively, compare with the value at the PDE of 10%. As for PGA-314, the avalanche builds up freely until the active-quenching circuit starts to quench it after a fixed delay determined by the total delay of the components in the feedback loop of the circuit. When the excess bias was high, the avalanche current of PGA-314 develops rapidly during the delay, where the carriers outnumber those generated during the slow quenching process for the NFAD. Consequently, the increase of the carriers for PGA-314 were 66% and 192% at the PDE of 15% and 20%, respectively, compared with the value at 10%, as shown in Fig. 7(d). Such non-linear rising of the number of carriers plus higher-order afterpulsing effect has lead to an acute rise of the TAP at high PDE for PGA-314.

Nevertheless, it should be mentioned that the minimum dead time for free-running standard InP-based SPAD was only 40 ns limited by our hardware [14]. Since the performance of standard

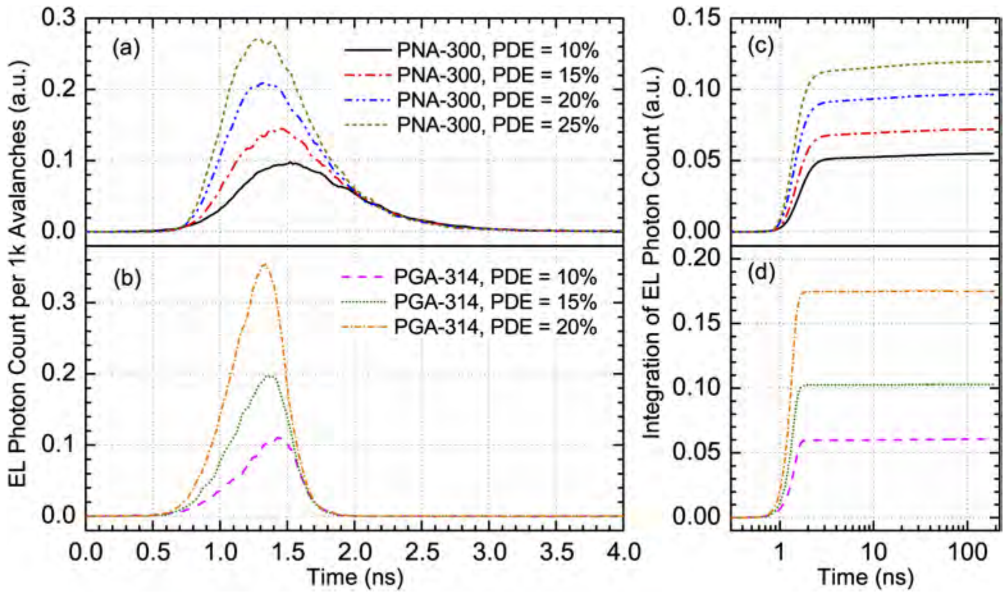

Fig. 7. Avalanche waveforms of PNA-300 (a) and PGA-314 (b) at various PDEs, 223 K, demonstrated by the electroluminescent photon count per 1000 avalanches. The integration of the counts of the waveforms for PNA-300 (c) and PGA-314 (d) over time indicates the relative change in avalanche carriers as the detection efficiency rises.

SPAD at low PDE was comparable to that of the NFAD, the standard SPAD is still possibly preferred if free-running operation with ultra-low dead time rather than high PDE is required.

5. Conclusion

In this paper, we have presented an active-quenching circuit specifically designed for the NFAD and its characterization. Electroluminescence experiments were conducted to show that active quenching was capable of facilitating both quenching and recovery of the NFAD by discharging and recharging the junction capacitor actively. The reduction in the avalanche carriers, the afterpulse probability and dead time has contributed to a minimum usable dead time was down to 80 ns with a TAP of 20.4% at the PDE of 10%, 1550 nm, 223 K, where the DCR was as low as 918 Hz. Compared with a standard SPAD aiming at similar applications, the proposed detector with NFAD has demonstrated much better overall performance, particularly at relatively high PDE. In general, this compact detector is especially suitable for use in lidar applications with its low afterpulsing, low dead-time, and low DCR features.

Funding. Applied Research Foundation for Post-doctoral Researchers in Qingdao City.

Acknowledgments. We would like to thank Dr. Shuzhen Fan for useful discussions.

Disclosures. The authors declare no conflicts of interest.

References

1. A. M. Pawlikowska, A. Halimi, R. A. Lamb, and G. S. Buller, "Single-photon three-dimensional imaging at up to 10 kilometers range," Opt. Express **25**(10), 11919–11931 (2017).
2. Z.-P. Li, X. Huang, Y. Cao, B. Wang, Y.-H. Li, W. Jin, C. Yu, J. Zhang, Q. Zhang, C.-Z. Peng, F. Xu, and J.-W. Pan, "Single-photon computational 3d imaging at 45 km," Photonics Res. **8**(9), 1532–1540 (2020).
3. P. Hu, H. Li, L. You, H. Wang, Y. Xiao, J. Huang, X. Yang, W. Zhang, Z. Wang, and X. Xie, "Detecting single infrared photons toward optimal system detection efficiency," Opt. Express **28**(24), 36884–36891 (2020).

Optics EXPRESS

4. N. Yao, Q. Yao, X.-P. Xie, Y. Liu, P. Xu, W. Fang, M.-Y. Zheng, J. Fan, Q. Zhang, L. Tong, and J.-W. Pan, "Optimizing up-conversion single-photon detectors for quantum key distribution," Opt. Express **28**(17), 25123–25133 (2020).
5. K. Kuzmenko, P. Vines, A. Halimi, R. J. Collins, A. Maccarone, A. McCarthy, Z. M. Greener, J. Kirdoda, D. C. S. Dumas, L. F. Llin, M. M. Mirza, R. W. Millar, D. J. Paul, and G. S. Buller, "3D LIDAR imaging using Ge-on-Si single-photon avalanche diode detectors," Opt. Express **28**(2), 1330–1344 (2020).
6. P. Vines, K. Kuzmenko, J. Kirdoda, D. C. S. Dumas, M. M. Mirza, R. W. Millar, D. J. Paul, and G. S. Buller, "High performance planar germanium-on-silicon single-photon avalanche diode detectors," Nat. Commun. **10**(1), 1086 (2019).
7. L. F. Llin, J. Kirdoda, F. Thorburn, L. L. Huddleston, Z. M. Greener, K. Kuzmenko, P. Vines, D. C. S. Dumas, R. W. Millar, G. S. Buller, and D. J. Paul, "High sensitivity ge-on-si single-photon avalanche diode detectors," Opt. Lett. **45**(23), 6406–6409 (2020).
8. C. Yu, J. Qiu, H. Xia, X. Dou, J. Zhang, and J.-W. Pan, "Compact and lightweight 1.5 μm lidar with a multi-mode fiber coupling free-running ingaas/inp single-photon detector," Rev. Sci. Instrum. **89**(10), 103106 (2018).
9. J. Zhang, M. A. Itzler, H. Zbinden, and J.-W. Pan, "Advances in InGaAs/InP single-photon detector systems for quantum communication," Light: Sci. Appl. **4**(5), e286 (2015).
10. M. A. Itzler, X. Jiang, M. Entwistle, K. Slomkowski, A. Tosi, F. Acerbi, F. Zappa, and S. Cova, "Advances in InGaAsP-based avalanche diode single photon detectors," J. Mod. Opt. **58**(3-4), 174–200 (2011).
11. T. Lunghi, C. Barreiro, O. Guinnard, R. Houlmann, X. Jiang, M. A. Itzler, and H. Zbinden, "Free-running single-photon detection based on a negative feedback InGaAs APD," J. Mod. Opt. **59**(17), 1481–1488 (2012).
12. M. Sanzaro, N. Calandri, A. Ruggeri, and A. Tosi, "InGaAs/InP SPAD with monolithically integrated Zinc-diffused resistor," IEEE J. Quantum Electron. **52**(7), 1–7 (2016).
13. R. T. Thew, D. Stucki, J.-D. Gautier, H. Zbinden, and A. Rochas, "Free-running InGaAs/InP avalanche photodiode with active quenching for single photon counting at telecom wavelengths," Appl. Phys. Lett. **91**(20), 201114 (2007).
14. J. Liu, T. Zhang, Y. Li, L. Ding, J. Tao, Y. Wang, Q. Wang, and J. Fang, "Design and characterization of free-running InGaAsP single-photon detector with active-quenching technique," J. Appl. Phys. **122**(1), 013104 (2017).
15. B. Korzh, T. Lunghi, K. Kuzmenko, G. Boso, and H. Zbinden, "Afterpulsing studies of low-noise InGaAs/InP single-photon negative-feedback avalanche diodes," J. Mod. Opt. **62**(14), 1151–1157 (2015).
16. B. Korzh, N. Walenta, T. Lunghi, N. Gisin, and H. Zbinden, "Free-running InGaAs single-photon detector with 1 dark count per second at 10% efficiency," Appl. Phys. Lett. **104**(8), 081108 (2014).
17. C. Yu, M. Shangguan, H. Xia, J. Zhang, X. Dou, and J.-W. Pan, "Fully integrated free-running InGaAs/InP single-photon detector for accurate lidar applications," Opt. Express **25**(13), 14611–14620 (2017).
18. X. Jiang, M. A. Itzler, K. O'Donnell, M. Entwistle, and K. Slomkowski, "Shortwave infrared negative feedback avalanche diodes and solid-state photomultipliers," Opt. Eng. **53**(8), 081908 (2014).
19. X. Jiang, M. Itzler, K. O'Donnell, M. Entwistle, M. Owens, K. Slomkowski, and S. Rangwala, "Inp-based single-photon detectors and geiger-mode apd arrays for quantum communications applications," IEEE J. Sel. Topics Quantum Electron. **21**(3), 5–16 (2015).
20. M. A. Itzler, X. Jiang, B. Nyman, and K. Slomkowski, "InP based negative feedback avalanche diodes," Proc. SPIE **7222**, 72221K (2009).
21. F. Acerbi, A. D. Frera, A. Tosi, and F. Zappa, "Fast active quenching circuit for reducing avalanche charge and afterpulsing in InGaAs/InP single-photon avalanche diode," IEEE J. Quantum Electron. **49**(7), 563–569 (2013).
22. M. A. Itzler, X. Jiang, B. M. Onat, and K. Slomkowski, "Progress in self-quenching InP-based single photon detectors," Proc. SPIE **7608**, 760829 (2010).
23. D. A. Ramirez, M. M. Hayat, G. J. Rees, X. Jiang, and M. A. Itzler, "New perspective on passively quenched single photon avalanche diodes: effect of feedback on impact ionization," Opt. Express **20**(2), 1512–1529 (2012).
24. J. Liu, Y. Li, L. Ding, Y. Wang, T. Zhang, Q. Wang, and J. Fang, "Fast Active-Quenching Circuit for Free-Running InGaAs(P)/InP Single-Photon Avalanche Diodes," IEEE J. Quantum Electron. **52**(10), 1–6 (2016).
25. K. E. Jensen, P. I. Hopman, E. K. Duerr, E. A. Dauler, J. P. Donnelly, S. H. Groves, L. J. Mahoney, K. A. McIntosh, K. M. Molvar, A. Napoleone, D. C. Oakley, S. Verghese, C. J. Vineis, and R. D. Younger, "Afterpulsing in Geiger-mode avalanche photodiodes for 1.06 μm wavelength," Appl. Phys. Lett. **88**(13), 133503 (2006).
26. F.-X. Wang, W. Chen, Y.-P. Li, D.-Y. He, C. Wang, Y.-G. Han, S. Wang, Z.-Q. Yin, and Z.-F. Han, "Non-Markovian Property of Afterpulsing Effect in Single-Photon Avalanche Detector," J. Lightwave Technol. **34**(15), 3610–3615 (2016).
27. M. M. Hayat, D. A. Ramirez, G. J. Rees, and M. A. Itzler, "Modeling negative feedback in single-photon avalanche diodes," Proc. SPIE **7681**, 76810W (2010).